Good vibrations: oscillatory phase shapes perception

T. Neuling[a], S. Rach[a], S. Wagner[b], C. H. Wolters[b], C. S. Herrmann[a,c,*]

[a] *Experimental Psychology Lab, University of Oldenburg, Ammerländer Heerstr. 114-118, 26111, Oldenburg, Germany*
[b] *Institute for Biomagnetism and Biosignalanalysis, University of Münster, Malmedyweg 15, 48149, Münster, Germany*
[c] *Research Center Neurosensory Science, University of Oldenburg, Ammerländer Heerstr. 114-118, 26111, Oldenburg, Germany*

Abstract

In the current study, we provide compelling evidence to answer the long-standing question whether perception is continuous or periodic. Spontaneous brain oscillations are assumed to be the underlying mechanism of periodic perception. Depending on the phase angle of the oscillations, an identical stimulus results in different perceptual outcomes. Past results, however, can only account for a correlation of perception with the phase of the ongoing brain oscillations. Therefore, it is desirable to demonstrate a causal relation between phase and perception. One way to address this question is to entrain spontaneous brain oscillations by applying an external oscillation and then demonstrate behavioral consequences of this oscillation. We conducted an auditory detection experiment with humans, recorded the electroencephalogram (EEG) concurrently and simultaneously applied oscillating transcranial direct current stimulation at 10 Hz (α-tDCS). Our approach revealed that detection thresholds were dependent on the phase of the oscillation that was entrained by α-tDCS. This behavioral effect was accompanied by an electrophysiological effect: α-power was enhanced after α-tDCS as compared to a pre-stimulation period.

By showing a causal relation between phase and perception, our results extend findings of previous studies that were only able to demonstrate a correlation. We found that manipulation of the phase resulted in different detection thresholds, which supports the notion that perception can be periodically modulated by oscillatory processes. This demonstrates that tDCS can serve as a tool in neuroscience to extend the knowledge of the functional significance of brain oscillations.

Keywords: tDCS, tACS, EEG, alpha, phase, perception

*Corresponding author
Email: christoph.herrmann@uni-oldenburg.de
Tel: +49 (0)441-798-4936
Fax: +49 (0)441-798-3865

1. Introduction

It is still a matter of debate whether brain oscillations indeed have a causal role in perception, cognition, and action, or are a mere epiphenomenon. Brain oscillations are believed to serve as an essential factor to code the temporal dynamics of our environment (Cohen, 2011). The phase of brain oscillations, in particular, carries temporal information in the millisecond range which is transferred and distributed within (Lakatos et al., 2008) and across (Varela et al., 2001) brain regions. The oscillatory phase represents brain states fluctuating between high and low cortical excitability (Engel et al., 2001; Lakatos et al., 2007), a concept proposed by Bishop (1932) over 75 years ago. Depending on that internal state, identical external events can result in different perceptual and behavioral outcomes. In particular, the phase of the α-rhythm (8–12 Hz) has been proposed to account for differences in reaction times (Callaway and Yeager, 1960), the perceptual fate of auditory (Rice and Hagstrom, 1989) and visual stimuli (Busch et al., 2009; Mathewson et al., 2009), as well as visual attention (Busch and VanRullen, 2010).

The latter results especially support the notion that perception is periodic, represented as a sequence of snapshots (Busch et al., 2009; Busch and VanRullen, 2010; Mathewson et al., 2009; Varela et al., 1981) rather than as a continuous stream, supporting a hypothesis proposed by VanRullen and Koch (2003). These studies, however, reflect only a correlation between perception and the phase of the ongoing EEG oscillations but not for a causal relation.

The question whether perception is periodic and if the periodicity is caused by the oscillatory phase can be addressed by entraining spontaneous brain oscillations through applying an external oscillation and subsequently demonstrating behavioral consequences of this oscillation (Sejnowski and Paulsen, 2006). Recently, techniques to stimulate the human cortex non-invasively have been developed that are capable of modulating the ongoing rhythmic brain activity (transcranial alternating current stimulation, tACS; e.g., Kanai et al., 2008; Zaehle et al., 2010), oscillating transcranial direct current stimulation, otDCS; e.g., Antal et al., 2008; Marshall et al., 2006, and rhythmic transcranial magnetic stimulation, rTMS; e.g. Klimesch et al., 2003; Romei et al., 2010, 2012; Thut et al., 2011). Most of these studies, however, are limited by only demonstrating either the effects of stimulation on behavior or changes in brain activity caused by the stimulation, but not both simultaneously. Only Marshall et al. (2006) demonstrated physiological and behavioral effects after rhythmic brain stimulation, but did not focus on the effect of oscillatory phase.

The present findings extend beyond previous studies by providing three lines of evidence for the effectiveness of otDCS applied at 10 Hz (α-tDCS): (1) an entrainment of ongoing brain oscillations in the applied frequency, (2) the modulation of the detection performance by the phase of the applied α-tDCS, and (3) simulation results demonstrating a super threshold current flow in the auditory cortex. In particular, evidences (1) and (2) reveal the first account of a causal oscillatory-phase-behavior dependence (Sejnowski and Paulsen, 2006) and support the notion that perception is periodic rather than continuous.

2. Materials & Methods

2.1. Participants

Twenty healthy, right-handed subjects (10 female) with a mean age of 25.9 ± 5.5 years participated in the study after providing written informed consent. Participants were medication-free at the time of the experiments. They reported no hearing deficits, presence or history of epilepsy, neurological or psychiatric disorders, cognitive impairments, intracranial metal or cochlear implants. Four participants were excluded due to insufficient behavioral data with performance that did not exceed a detection rate of 90 %. Sixteen subjects (7 female) with a mean age of 24.06 ± 2.5 years remained for data analysis. The experimental protocol was approved by the ethics committee of the University of Magdeburg and was conducted in accordance with the Declaration of Helsinki.

2.2. EEG

The experiment was performed in a dimly lit room with the participant seated in a recliner. The EEG was measured from 23 sintered Ag-AgCl electrodes mounted in an elastic cap (Easycap, Falk Minow, Munich, Germany) at scalp locations Fp1, Fp2, F7, F3, Fz, F4, F8, FT9, FT10, FC1, FC2, FC5, FC6, C3, C4, Cz, P3, P4, Pz, O1, O2, CP1, CP2 (according to the 10-10 system) referenced to the nose. Vertical electrooculogram was computed on the bipolar recording of Fp2 with respect to an electrode below the right eye. The ground electrode was positioned on the forehead at Fpz. Electrode resistance was kept below 10 kΩ. Signals were recorded using Brain Vision Recorder (Brain Products GmbH, Gilching, Germany). Signals were sampled at 1000 Hz and amplified in the range of ± 3.2768 mV at a resolution of 0.1 μV. Stimulus markers and EEG data were digitally stored on hard disk for further offline analysis.

2.3. Electrical stimulation

α-tDCS was applied via two saline-soaked sponge electrodes (5 × 7 cm) (Neuroconn, Ilmenau, Germany) attached bilaterally to the scalp at temporal locations (approximately at electrode locations T7 and T8) underneath the EEG recording cap. The impedance was kept below 10 kΩ. A direct current of 1 mA modulated by a sinusoidal current of 425 ± 81 μA was applied at 10 Hz using a battery-operated stimulator system (Eldith, Neuroconn, Ilmenau, Germany). The sinusoidal current was adjusted individually: we started at a level of 400 μA. If the subject indicated that the stimulation was uncomfortable we decreased the current in steps of 50 μA until the subject indicated that the level of stimulation was acceptable. If the subject indicated that the stimulation was comfortable, we increased the current in steps of 50 μA until the subject indicated that the level of stimulation was uncomfortable. Then we decreased the current until the subject indicated that the stimulation was acceptable. Each intensity step was applied for 20 seconds to familiarize the subject with the stimulation current. The oscillatory stimulation leads to opposite phases at the electrodes. That means the excitability phases are opposite to each other on each hemisphere which could corrupt the phase dependence of detection thresholds. Additionally, there is a left ear advantage for non-verbal auditory stimuli (Kimura, 1967). To compensate for that, we applied a 1 mA current to the anode. This leads to increased excitation below the anode which was placed on the right hemisphere and decreased excitation below the cathode which was placed on the left hemisphere (Nitsche and Paulus, 2000).

2.4. Design

The electrical stimulation was carried out in two sessions on separate days to keep the duration of the tDCS stimulation below 25 minutes per day. The experimental procedure is illustrated in Fig. 1A and was the same for both days. After the EEG and TES electrodes were applied, the individual hearing threshold was determined for each ear of each subject. During the experiment, subjects were to detect 500 Hz tones of 10 ms duration (ISI 1.5–2.5 s) embedded in continuous, band-limited white noise with seven different signal-to-noise ratios (SNR: from -4 dB to 8 dB). The noise was created by equally distributed frequencies (0–500 Hz) with random phases sampled at 1000 Hz. The sounds were delivered binaurally using insert earphones (EARTone 3A) and a calibrated attenuator (Tucker-Davis Technologies, Alachua, FL, USA; model PA5). The timing of the stimuli was arranged relative to the α-tDCS to present the stimuli in specific phase bins. The noise was presented at a sound level of 60 dB above individual hearing threshold. Participants were instructed to indicate detection of the signal by pressing a button. The detection task was divided into four blocks of seven minutes: the first block without α-tDCS and three blocks with α-tDCS. EEG was recorded for three minutes before the first block (*pre*-EEG) and after the last block (*post*-EEG).

2.5. Data analysis

Data analysis was performed using MATLAB 7 (The MathWorks Inc, Natick, MA, USA) and Python 2.6 (http://www.python.org).

2.5.1. Behavioral data

The first step in analyzing the behavioral data was to subdivide the data from the blocks with α-tDCS stimulation into six phase bins of 60°, according to the phase angle of the sine of the α-tDCS stimulation (Fig. 1B). The data without α-tDCS stimulation from the first block served as baseline condition. Next, for each participant, the psychometric function

$$F_{a,b,\gamma,\lambda}(x) = \gamma + (1 - \lambda - \gamma) \cdot \frac{1}{1 + e^{\frac{-(x-a)}{b}}}, \tag{1}$$

with threshold a, slope b, guessing rate γ, and lapsing rate λ was estimated (Fig. 1C) for the behavioral data of each of the 6 phase bins and the baseline condition (x being the SNR at which the sound was presented). Parameters were estimated simultaneously for all seven conditions using the following constraints: for each condition, one threshold parameter a was estimated; whereas slope b, guessing rate γ, and lapsing rate λ were estimated once for all of the seven conditions. Parameter estimation minimized the squared residuals using the MatLab routine FMINSEARCH. Further analyses used the threshold parameter a from each subject. Because of differences in individual performance variations, the detection threshold was normalized for each observer by subtracting the detection threshold without α-tDCS for that observer from the threshold for each phase bin. Due to inter-individual differences in cortical anatomy, the exact phase at which the individual performance was highest and lowest varied slightly among subjects which makes phase alignment mandatory (Busch et al., 2009; Busch and VanRullen, 2010). Therefore, the phase distributions for each participant were aligned so that the zero crossing was at a phase angle of 180°. For further computation the aligned phase distributions were

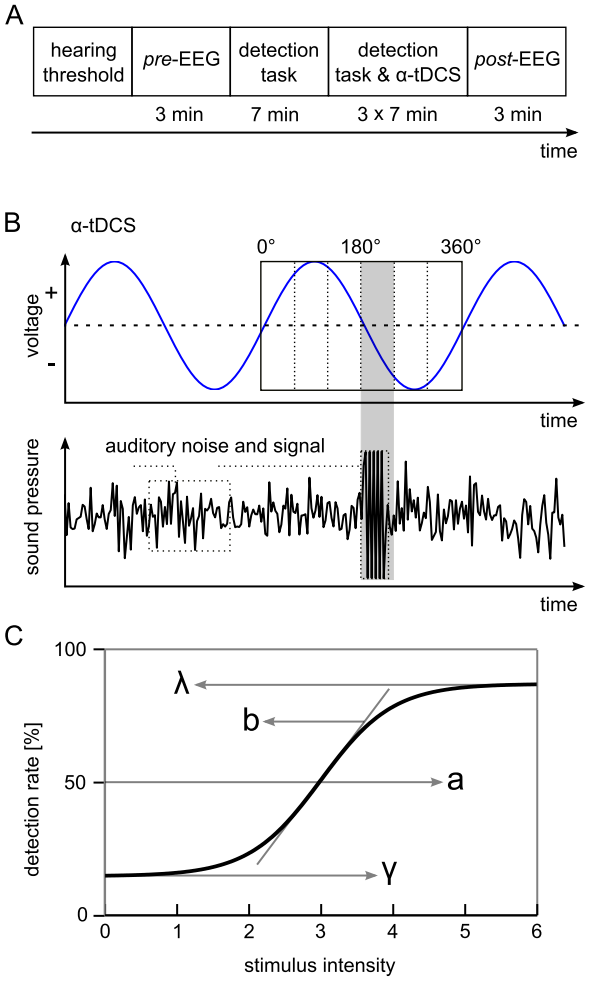

Figure 1: **Experimental procedures** (A) Timeline of the experimental procedure. The experiment started with determining the hearing threshold followed by a three minute EEG measurement (*pre*-EEG). Subsequently, the subjects performed a signal detection task for four blocks of seven minutes, where the first seven minutes were without electrical stimulation. After the electrical stimulation, another three minutes of EEG were measured (*post*-EEG). (B) α-tDCS and auditory signal: The auditory signal was presented in one of seven different signal-to-noise ratios in one of six different phase bins. This is an example of the auditory signal presented within the fourth phase bin. (C) Psychometric function. Four parameters specify the shape of the psychometric function which is a logistic function. Parameters a and b represent the threshold and slope, respectively. Parameter γ, the lower asymptote, is the guessing rate and can be interpreted as the probability that the observer only guesses when indicating that the stimulus was observed. Parameter λ, the upper asymptote, is the lapsing rate and can be interpreted as the probability that the observer misses the stimulus. For every psychometric function for a certain subject, parameters b, λ, and γ were estimated once for all of the seven conditions whereas a, the threshold, was individually estimated for each function. Stimulus intensity unit is the SNR of the auditory signal and the noise.

used. For statistical analysis, the thresholds were entered into an analysis of variance (ANOVA) with phase bin as a factor with six levels. Subsequently, post-hoc t tests (Bonferroni corrected) were performed. To test the phases for their influence on detection performance, we applied the analysis introduced by Naue et al. (2011). Assuming the sinusoidal model

$$y = g \cdot sin(h \cdot 2\pi(t + c)), \tag{2}$$

a nonlinear regression analysis was performed. The routine to fit the parameters was initialized with random start values. The parameters were limited by the following constraints: $g \in$ [-1, 1], $h \in$ [8, 12], $c \in$ [-π, π]. To test for significance, a Student's t test was performed on parameter g. The null hypothesis assumed g to be zero, i.e., representing a horizontal line that would indicate no modulation by phase.

2.5.2. EEG data

Data analysis was based upon the approach introduced by Zaehle et al. (2010). Each of the two datasets (*pre*-EEG, *post*-EEG) from each participant was split into 180 one-second segments. Segments containing artifacts (eye blinks, muscle activity) were rejected from further analysis. The first 100 segments of each dataset without artifacts were included in subsequent analysis. After subtracting the mean value of each segment to avoid DC distortion of the spectra at 0 Hz, a fast Fourier transform (FFT) was applied on each segment and the resulting 100 spectra for each dataset were averaged. The parieto-occipital electrode Pz was chosen for analysis. To evaluate power changes in the range of the α-frequency (8–12 Hz), the individual peak spectral amplitudes were calculated and entered into a t test. Additionally, we analyzed frequency bands above (*upper band*, 13–15 Hz) and below (*lower band*, 5–7 Hz) the α-band. In order to account for individual differences, the power data were normalized to the α-power of the pre-EEG measurement.

2.5.3. tDCS simulation

For a tDCS simulation study, a realistic finite element (FE) head model was generated from a T1-weighted, a T2-weighted and a diffusion-tensor-(DT-) magnetic resonance image (MRI) of a healthy 26 year old male subject. In a first step, the T2-MRI was rigidly registered onto the T1-MRI using a mutual information based cost-function (Jenkinson and Smith, 2001). Segmentation into tissue compartments skin, skull compacta, skull spongiosa, cerebrospinal fluid (CSF), brain grey (GM) and white matter (WM) was then performed using the FSL software (http://www.fmrib.ox.ac.uk/fsl) (Jenkinson et al., 2005; Smith, 2002; Zhang et al., 2001). Segmentation started with the generation of initial masks for skin, inner and outer skull and brain using both T1- and T2-MRI. In a second step, the T1-MRI served for GM and WM segmentation, while the T2-MRI allowed for a segmentation of skull compacta, skull spongiosa and CSF space. For the compartments skin, skull compacta, skull spongiosa and CSF, we used the isotropic conductivity values of 0.43 S/m, 0.007 S/m, 0.025 S/m and 1.79 S/m, resp. (Akhtari et al., 2002; Baumann et al., 1997; Dannhauer et al., 2011). For the modeling of white matter conductivity anisotropy, the diffusion-weighted images were first artifact-corrected using our reversed-gradient approach introduced in (Olesch et al., 2010). Diffusion tensors were then determined and the result was registered onto the structural images using the

FSL routine vecreg (http://fsl.fmrib.ox.ac.uk/fsl/fdt/fdt_utils.html#vecreg). In a last step, the conductivity anisotropy in GM and WM was computed from the registered DTI using an effective medium approach as described by us (Rullmann et al., 2009) and presented in (Tuch et al., 2001).

Two electrode patches with a size of 7×5 cm and thickness of 4 mm, positioned on the head surface under professional guidance, are modeled over the auditory cortices (see Fig. 2A). A total current of 1 mA is injected at the red colored patch (anode) and removed at the blue colored one (cathode). For field modeling of this stimulation throughout the volume conductor, a quasistatic approximation of Maxwell's equations (Plonsey and Heppner, 1967) was used, resulting in a Laplace equation for the electric potential Φ with inhomogeneous Neumann boundary conditions at the head surface. An isoparametric FE approach is used for the computation of Φ in a 1mm geometry-adapted hexahedral mesh (Wolters et al., 2007b,a), resulting in a large sparse linear equation system with 2.255 million unknowns, which is solved using an algebraic multigrid preconditioned conjugate gradient approach (Lew et al., 2009; Wolters et al., 2002). In a last step, the current density $J = \sigma\ \mathrm{grad}\Phi$ is computed with σ being the 3×3 conductivity tensor. For simulation, we used our software SimBio (http://www.mrt.uni-jena.de). In Fig. 2B and 2C a coronal slice of the current density distribution through the auditory cortex is presented. The amplitude of J is coded by means of a color-scale. Fig. 2B was computed in the 1 mm geometry-adapted hexahedral mesh, but for the purpose of clear visualization the resulting vector field is only shown on a thinned version of this mesh, i.e., we only present the vector in the middle of each 4 mm x 4 mm block. A detailed view of the vector field in Heschl's gyrus in full resolution of 1 mm is shown in Fig. 2C. The upper subfigure 2C shows the current density in the CSF, GM and WM compartments and the lower subfigure only in the GM and WM compartments. For visualization, the software SciRun (http://www.sci.utah.edu/cibc/software/106-scirun.html) was used.

3. Results

3.1. Behavioral data

The psychometric functions obtained after fitting the behavioral data differ for the 7 conditions. Figs. 3A/B illustrate that the psychometric function shifts depend on the phase bin during which the stimuli were presented. With respect to baseline, there are phases with higher detection thresholds and phases with lower detection thresholds.

This finding was confirmed by an ANOVA with the factor phase which was comprised of 6 bins. It revealed a significant main effect of phase bin ($F_{5,14} = 8.55$, $P < 0.001$). A t test for independent samples revealed that the threshold was significantly higher when the stimuli where presented in the positive half-wave compared to the threshold for stimuli presented in the negative half-wave ($t_{47} = 8.96$, $P < 0.001$), which is illustrated in Fig. 3D. The sine waves, which were fitted to the behavioral data, are depicted in Fig. 3E/F. A t test on the parameter g (amplitude) revealed that g ($t_{15} = 10.34$, $P < 0.001$) was significantly different from 0, demonstrating that the sinusoidal modulation by phase was significant. How the detection performance is modulated by the oscillation is illustrated with the model in Fig. 3C. The sinusoidal pattern of the stimulation shapes the detection performance accordingly.

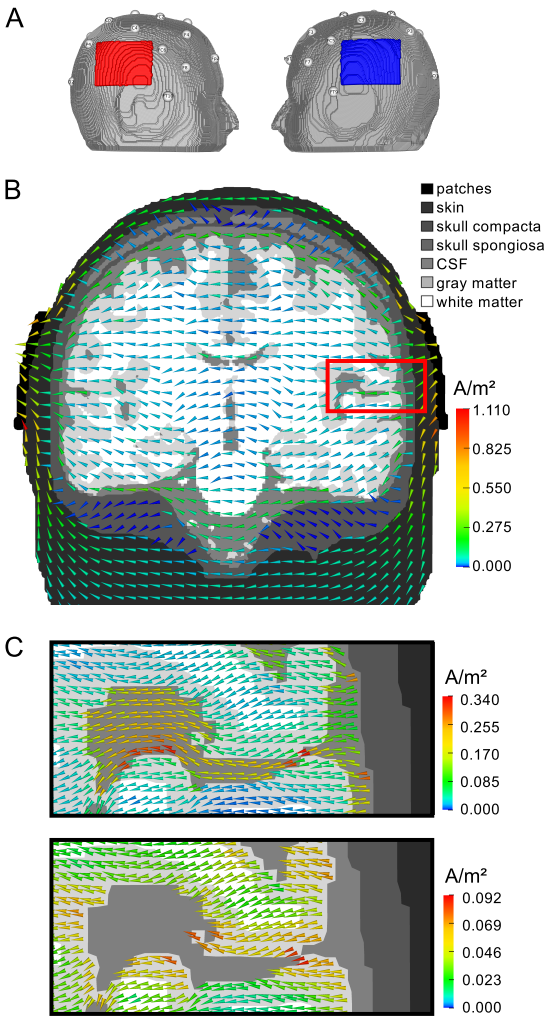

Figure 2: **tDCS simulation**.(A) Location of the stimulation electrodes (red: anode, blue: cathode) on the head surface. (B) Coronal slice of the vector field of the simulated current density through the head. The highlighted area (red box) depicts Heschl's gyrus. (C) Detailed view of Heschl's gyrus. Different scales are used to point out the current flow in the different tissue compartments. The upper figure highlights the current flow in the CSF, the lower figure highlights the current flow in the gray and white matter.

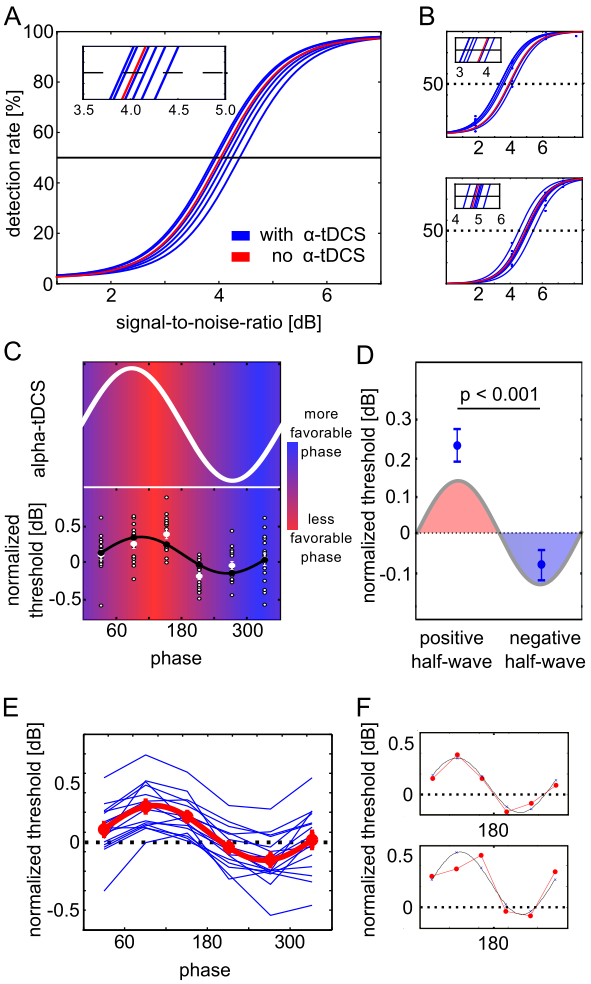

Figure 3: **Behavioral results** (A/B) Phase-specific psychometric functions. Each blue curve corresponds to one of the six phase bins. The red curve represents the baseline performance. The intersections with the threshold at 50% correspond to the threshold parameter. (A) Averaged psychometric functions for each of the six phase bins. Parameters were averaged for illustration purposes. (B) Psychometric functions for each of the six phase bins for two exemplary subjects. Raw data points (stars) and fitted functions for each of the six phase bins. (C) Detection threshold shaped by α-tDCS. The detection threshold is modulated by the phase of the α-tDCS. The upper sine waves illustrate the α-tDCS. The lower black curve shows the relative difference from the baseline of the fits for the averaged normalized detection performance $\pm$ standard error of the mean (s.e.m.) for each phase bin. White points denote individual data points for each participant. The thick white points represent the average of the behavioral data. The color of the shaded region represents the transition from less to more favorable phases. A normalized threshold refers to the change in SNR necessary to detect a sound as compared to a condition without α-tDCS, i.e. +0.5 indicates that sounds need to have a higher SNR to be detected (worse performance). This scale applies also to Figs. D-F. (D) Normalized detection thresholds for the positive half-wave of the sine of the α-tDCS compared to the negative half-wave. Group averages $\pm$ s.e.m. are shown. The relative difference from baseline of the normalized detection performance for each phase bin is illustrated. (E/F) Sine fits of the behavioral data. (E) Blue lines represent the fits for single subject data. The red line shows the average fit in a higher resolution for illustration purposes. Red dots denote the mean of the fitted data $\pm$s.e.m. (F) Sine fits for two exemplary subjects. The red line shows the raw data and the black line shows the fitted sine wave.

3.2. Electrophysiological data

The FFT power spectra of electrode Pz (Fig. 4A) demonstrated an enhancement of the individual α-power after α-tDCS. The comparison of the individual α-power before (*pre*) and after (*post*) α stimulation revealed an average increase in power (Fig. 4B) by 7%. The amplitude of the peak in the α-range (8–12 Hz) was larger for the EEG measurement after the α-tDCS than before, as revealed by a t-test for paired samples (t_{31}= -2.01, P = 0.026, one sided). This increase was no broadband enhancement of spectral power. In the *upper* (12–14 Hz, t_{31}= 0.94, P = 0.18, one sided) and *lower* (6–8 Hz, t_{31}= -0.25, P = 0.40, one sided) frequency bands no increase in power was observed. Additionally, a power increase in the δ-range (1–4 Hz) could be observed (t_{31}= -3.26, P = 0.001, one sided).

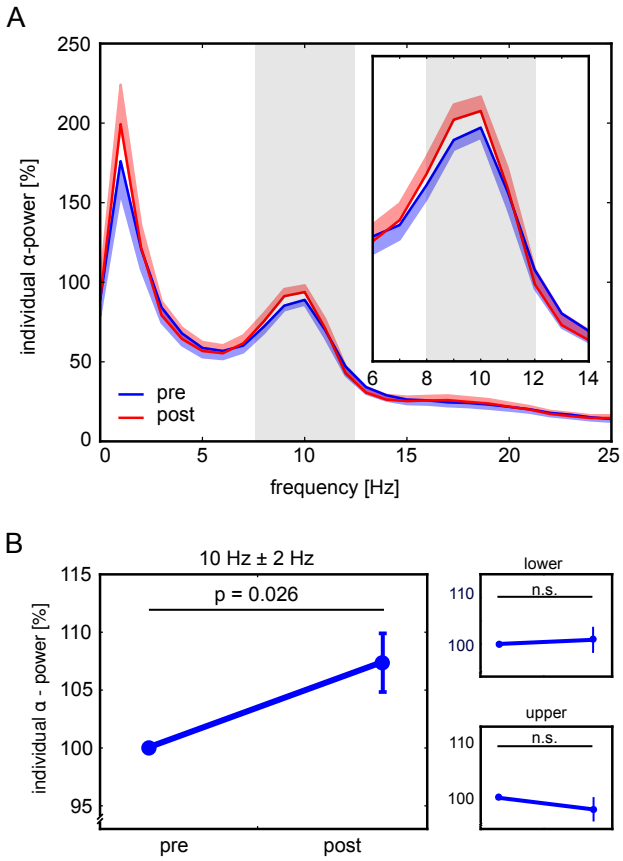

Figure 4: **EEG results**. (A) Averaged EEG activity. FFT power spectra for the 3 minutes before (*pre*, blue) and after (*post*, red) α-tDCS. Hundred percent correspond to the peak power in the α-range in the pre-stimulation period. Shaded regions show the s.e.m. (B) Mean individual peak amplitude in the α-range. From the pre- to the post-stimulation EEG measurement, the power of the peak in the δ- (0–4 Hz) and α-range (8–12 Hz) increased. In the upper(13–15 Hz)- and lower (5–7 Hz)-frequency bands with respect to the stimulation frequency, the power did not increase. Data are normalized to the peak power before α-tDCS. Group averages ± s.e.m. are shown.

3.3. Electrical modeling

Recent studies have demonstrated that the intracranial current flow of tDCS can be modelled in detail when using realistic head models (Sadleir et al., 2010; Wagner et al., 2007). We have extended this approach to model the current flow of our experiment. Our simulation demonstrates how the current density is distributed in the different tissue compartments. In Fig. 2B an overall view of the vector field is presented on a coronal slice through the auditory cortex, for the purpose of clear visualization on a thinned version of the underlying 1 mm computational grid. The highest current density can be observed at the edges of the electrode patches and a large amount of current density is distributed tangentially along the skin compartment (from the anode to the cathode). Due to the low conductivity of the skull compartments (compacta and spongiosa), mainly radially oriented currents with low amplitude flow through the skull. The highly conductive cerebrospinal fluid (CSF) tunnels a large amount of current density into the depth of Heschl's gyrus, as can be observed in Fig. 2C (full 1 mm resolution).

4. Discussion

In the present study, we demonstrated that the performance in an auditory signal detection task is modulated by the phase of oscillations entrained by α-tDCS. By altering detection thresholds through selectively interfering with brain oscillations, we established a causal link between oscillations and perception (Sejnowski and Paulsen, 2006), extending previous studies that only provided correlational evidence (Busch et al., 2009; Busch and VanRullen, 2010; Mathewson et al., 2009). Our modelling study revealed that transcranial electrical stimulation (TES) caused increased current amplitudes in Heschl's gyrus which explains the observed electrophysiological effects.

These results answer the question whether a weak current as applied with α-tDCS is able to influence the activity of cortical neurons in the human brain, resulting in an altered auditory perception. In our modelling study we demonstrated that TES can lead to significant current flow inside the human cortex, despite a large amount of the α-tDCS current being short-circuited by the well-conducting skin (Holdefer et al., 2006). Intracranial electric stimulation of neurons in animals has demonstrated that axons and especially the axon hillock are sensitive to this kind of stimulation due to the high number of voltage-sensitive Na ion channels (Nowak and Bullier, 1998). Francis et al. (2003) were able to demonstrate that electric fields of 140 μV/mm are sufficient to increase the firing rate of single neurons (i.e., super-threshold stimulation). Miranda et al. (2006) used an isotropic spherical head model to demonstrate that 2.0 mA of tDCS result in 0.1 A/m^2 corresponding to an electric field of 220 μV/mm. Our anisotropic simulation revealed an electric field of 275 μV/mm in Heschl's gyrus, which can be considered super-threshold. However, even if the stimulation had been sub-threshold, the phenomenon of stochastic resonance (McDonnell and Abbott, 2009) could explain the observed effects. If the external oscillation leads to fluctuations of the neurons' membrane voltage of around 100 μV, this oscillation still drives the neuron into more depolarized and more hyperpolarized states than without this stimulation. Thus, input arriving from other neurons during this slightly more depolarized phase makes a neuron more likely to fire than input arriving during slightly more hyperpolarized phases.

While most previous studies on the dependency of perception upon phase investigated the visual domain, Rice and Hagstrom (1989) reported an effect of the α-phase in an

auditory detection task. The EEG was recorded above the temporal cortex, similar to the position of our stimulation electrodes. They observed a significant difference in signal-detection performance between the negative and the positive peaks of the recorded α-oscillation. The present data replicate these results.

It may seem surprising that α-oscillations are that crucial for auditory perception, since the sources for the α-generation are usually found in posterior brain areas (Rodin and Rodin, 1995). However, Nunez et al. (2001) reported local sources of the cerebral α-rhythm to include the auditory cortex. Furthermore, Weisz et al. (2011) presented conclusive evidence for the functional significance of auditory alpha-generators. Thus, if the α-tDCS is applied to affect the auditory sources of α-oscillations this should result in a modulation of auditory performance (Thut and Miniussi, 2009). In the present study, the stimulation electrodes were attached above the temporal cortex and overlaid the auditory cortex. According to modeling approaches of others (Holdefer et al., 2006) and our own simulation, this electrode configuration leads to current pathways primarily affecting the auditory cortex.

Our EEG results show that the α-tDCS modulated the ongoing rhythmic brain activity in a frequency specific way. By applying an oscillation at a biologically relevant frequency, neurons with that intrinsic frequency preference can be forced to resonate (Hutcheon and Yarom, 2000). That leads to the assumption that neurons with a preferred frequency in the α-range will be entrained by the induced oscillation. Even though the α-tDCS in our study lasted for 20 minutes, the power within the α-range only increased moderately compared to the results of similar studies (Marshall et al., 2006, Zaehle et al., 2010). Those studies, however, differed from the current study in important ways. Marshall et al. (2006) also applied otDCS (at different stimulation sites) and observed an increase in δ-power after applying δ-tDCS, but no θ-increase after θ-tDCS. Zaehle et al. (2010) used tACS at the individual α-frequency of their participants, whereas we always used 10 Hz as the stimulation frequency. This might account for the difference in magnitude of the α-enhancement: 7 % in the current study compared to 14 % observed by Zaehle et al. Furthermore, their electrodes were placed bilaterally at parieto-occipital locations, while we stimulated temporal regions. According to Nunez et al. (2001), α-oscillations are much more prominent in parieto-occipital regions than in temporal areas. Thus, if more neurons are sensitive to α-oscillations in a specific region, this could explain why Zaehle et al. (2010) reported a greater increase in α-power than we did. In general, it is known that even slight differences in aspects like electrode arrangement (Feira et al., 2009), stimulation technique (Antal et al., 2008), stimulation intensity (Kanai et al., 2008, 2010), and frequency (Kanai et al., 2008; Marshall et al., 2006) can yield surprisingly different results. Further investigation is required to discern how the aforementioned aspects specifically affect the EEG.

A rather unexpected result was the observed increase in δ-power. A potential explanation could be the fact that our stimulation comprised DC as well as AC currents. It has repeatedly been demonstrated that tDCS can modulate EEG δ-oscillations (Ardolino et al., 2005; Keeser et al., 2011). However, in those studies either an enhancement or a reduction of δ-activity was observed under cathodal or anodal electrodes, respectively. For the analysis of our midline electrode (Pz), one would thus expect that the two effects cancel each other out, since the cathodally stimulated left cortex and the anodally stimulated right cortex contribute equally to this electrode location. Therefore, we would like to propose a more interesting albeit more speculative interpretation based on the

interaction of δ- and α-oscillations. Cross-frequency analyses demonstrated a functional coupling of these two frequencies, i.e. the phase of δ-activity can modulate the amplitude of faster wide-band activity that comprises the α-frequency band (Lakatos et al., 2008) or narrow-band activity explicitly in the α-frequency band (Cohen, 2009). In a previous stimulation-experiment, Marshall et al. (2006) used δ-tDCS and found an increase in δ- as well as α-power. If our increase of EEG δ-activity would be a result of the increased α-activity entrained by α-tDCS, this would open new perspectives for cross-frequency tACS/otDCS which would at the same time circumvent the EEG-artefact of the stimulation.

Even though the modulation of the auditory detection threshold by the phase of the induced α-oscillations is rather modest, it confirms theories about a cyclic periodicity in perception (Busch et al., 2009; Mathewson et al., 2009; Rice and Hagstrom, 1989; Schroeder and Lakatos, 2009; VanRullen and Koch, 2003; Varela et al., 1981). In addition, the results of this study were based upon the detection performance of the observers across separate sessions, which demonstrates the reliability of the results. The magnitude of the α-phase effect should not be overestimated, since other factors, such as oscillatory power (Busch et al., 2009; Hanslmayr et al., 2007), contribute to perception as well. Indeed, only if the α-power is high can a phase effect be observed, whereas the same effect is not observed when α-power is low (Mathewson et al., 2009). The α-phase also accounted for variations in auditory event-related potentials (Barry et al., 2004) and were interpreted as reflecting preferred brain states that facilitate processing of incoming stimuli.

Studies probing the causal role of intrinsic brain activity can be very fruitful for a better understanding of ongoing rhythmic activity and how it relates to perception and cognitive processes. Driving brain oscillations by oscillating transcranial electrical stimulation to specifically entrain brain oscillations of that frequency can serve as a new tool for neuroscientists. It will be possible to modulate oscillations and to test behavioral correlates of brain oscillations in order to demonstrate causality. The novel approach we used in our study not only confirmed that brain oscillations can be increased in a frequency specific manner, but also that the behavioral consequences of the fine-grained temporal dynamics of the oscillations can be uncovered, as shown by the phase-behavior dependence. Furthermore, oscillating currents could be used to treat psychiatric diseases that are associated with disturbed brain oscillations (Herrmann and Demiralp, 2005; Uhlhaas et al., 2008).

Our results demonstrate, for the first time, a direct causal relationship between the phase of an entrained oscillation and auditory signal-detection performance. This result further extends the functional significance of brain oscillations.

Acknowledgments. The authors would like to thank H. Kugel (Department of Clinical Radiology, University of Münster, Germany) for the measurement of the MRI, B. Lanfer, Ü. Aydin and J. Vorwerk (Institute for Biomagnetism and Biosignalanalysis, University of Münster, Germany) for the help in setting up the realistic head model, and C. Lavallee (Department for Experimental Psychology, University of Oldenburg, Germany) for proofreading the manuscript. This work was kindly supported by grants of the German Research foundation (DFG, SFB/TR 31 and HE3353/6–2) to CSH and (DFG, WO1425/3-1) to CHW.

5. References

Akhtari, M., Bryant, H. C., Marnelak, A. N., Flynn, E. R., Heller, L., Shih, J. J., Mandelkern, M., Matlachov, A., Ranken, D. M., Best, E. D., DiMauro, M. A., Lee, R. R., Sutherling, W. W., 2002. Conductivities of three-layer live human skull. Brain Topogr. 14, 151–167.

Antal, A., Boros, K., Poreisz, C., Chaieb, L., Terney, D., Paulus, W., 2008. Comparatively weak after-effects of transcranial alternating current stimulation (tACS) on cortical excitability in humans. Brain Stim. 1 (2), 97–105.

Ardolino, G., Boss, B., Barbieri, S., Priori, A., 2005. Non-synaptic mechanisms underlie the after-effects of cathodal transcutaneous direct current stimulation of the human brain. J. Physiol. 568(Pt2), 653–663.

Barry, R. J., Rushby, J. A., Johnstone, S. J., Clarke, A. R., Croft, R. J., Lawrence, C. A., 2004. Event-related potentials in the auditory oddball as a function of EEG alpha phase at stimulus onset. Clin. Neurophysiol. 115 (11), 2593–2601.

Baumann, S. B., Wozny, D. R., Kelly, S. K., Meno, F. M., 1997. The electrical conductivity of human cerebrospinal fluid at body temperature. IEEE Trans. Biomed. Eng. 44(3), 220–223.

Bishop, G. H., 1932. Cyclic changes in excitability of the optic pathway of the rabbit. Am. J. Physiol. 103, 213–224.

Busch, N., Dubois, J., VanRullen, R., 2009. The phase of ongoing EEG oscillations predicts visual perception. J. Neurosci. 17;29(24), 7869–7876.

Busch, N. A., VanRullen, R., 2010. Spontaneous EEG oscillations reveal periodic sampling of visual attention. Proc. Natl. Acad. Sci. 107 (37), 16048–16053.

Callaway, E., Yeager, C. L., 1960. Relationship between reaction time and electroencephalographic alpha phase. Science 132, 1765–1766.

Cohen, M. X., 2009. Oscillatory activity and phase-amplitude coupling in the human medial frontal cortex during decision making. J. Cogn. Neurosci. 21, 390–402.

Cohen, M. X., 2011. It's about time. Front. Hum. Neurosci. 5:2.

Dannhauer, M., Lanfer, B., Wolters, C. H., Knösche, T. R., 2011. Modeling of the human skull in EEG source analysis. Hum. Brain Mapp. 32 (9), 1383–1399.

Engel, A. K., Fries, P., Singer, W., 2001. Dynamic predictions: oscillations and synchrony in top-down processing. Nat. Rev. Neurosci. 2(10), 704–716.

Feira, P., Leal, A., Miranda, P. C., 2009. Comparing different electrode configurations using the 10-10 international system in tDCS: a finite element model analysis. Engineering in Medicine and Biology Society, 2009. EMBC 2009. Annual International Conference of the IEEE, 1596–1599.

Francis, J., Gluckman, B. J., Schiff, S. J., 2003. Sensitivity of neurons to weak electric fields. J. Neurosci. 23(19), 7255–7261.

Hanslmayr, S., Aslan, A., Staudigl, T., Klimesch, W., Herrmann, C. S., Bäuml, K.-H., 2007. Prestimulus oscillations predict visual perception performance between and within subjects. NeuroImage 37 (4), 1465–1473.

Herrmann, C. S., Demiralp, T., 2005. Human EEG gamma oscillations in neuropsychiatric disorders. Clin. Neurophysiol. 116 (12), 2719 – 2733.

Holdefer, R., Sadleir, R., Russell, M., 2006. Predicted current densities in the brain during transcranial electrical stimulation. Clin. Neurophysiol. 117 (6), 1388–1397.

Hutcheon, B., Yarom, Y., 2000. Resonance, oscillation and the intrinsic frequency preferences of neurons. Tr. Neurosci. 23 (5), 216–222.

Jenkinson, M., Pechaud, M., Smith, S., 2005. BET2: MR-based estimation of brain, skull and scalp surfaces. In: Eleventh Annual Meeting of the Organization for Human Brain Mapping.

Jenkinson, M., Smith, S., 2001. A global optimisation method for robust affine registration of brain images. Medical Image Analysis 5 (2), 143–156.

Kanai, R., Chaieb, L., Antal, A., Walsh, V., Paulus, W., 2008. Frequency-dependent electrical stimulation of the visual cortex. Curr. Biol. 18, 1839–1843.

Kanai, R., Paulus, W., Walsh, V., 2010. Transcranial alternating current stimulation (tACS) modulates cortical excitability as assessed by TMS-induced phosphene thresholds. Clin. Neurophysiol. 9, 1551–1554.

Keeser, D., Padberg, F., Reisinger, E., Pogarell, O., Kirsch, V., Palm, U., Karch, S., Möller, H. J., Nitsche, M. A., Mulert, C., 2011. Prefrontal direct current stimulation modulates resting EEG and event-related potentials in healthy subjects: a standardized low resolution tomography (sLORETA) study. NeuroImage 55(2), 644–657.

Kimura, D., 1967. Functional asymmetry of the brain in dichotic listening. Cortex III, 163–178.

Klimesch, W., Sauseng, P., Gerloff, C., 2003. Enhancing cognitive performance with repetitive transcranial magnetic stimulation at human individual alpha frequency. Europ. J. Neurosci. 17 (5), 1129–1133.
Lakatos, P., Chen, C.-M., O'Connell, M. N., Mills, A., Schroeder, C. E., 2007. Neuronal oscillations and multisensory interaction in primary auditory cortex. Neuron 53, 279–292.
Lakatos, P., Karmos, G., Mehta, A. D., Ulbert, I., Schroeder, C. E., 2008. Entrainment of neuronal oscillations as a mechanism of attentional selection. Science 320, 110–113.
Lew, S., Wolters, C. H., Röer, C., Dierkes, T., MacLeod, R. S., 2009. Accuracy and run-time comparison for different potential approaches and iterative solvers in finite element method based EEG source analysis. Appl. Numer. Math. 59(8), 1970–1988.
Marshall, L., Helgadottir, H., Mölle, M., Born, J., 2006. Boosting slow oscillations during sleep potentiates memory. Nature 444(7119), 610–613.
Mathewson, K. E., Gratton, G., Fabiani, M., Beck, D. M., Ro, T., 2009. To see or not to see: prestimulus alpha phase predicts visual awareness. J. Neurosci. 29(9), 2725–2732.
McDonnell, M. D., Abbott, D., 05 2009. What is stochastic resonance? definitions, misconceptions, debates, and its relevance to biology. PLoS Comput. Biol. 5 (5), e1000348.
Miranda, P. C., Lomarev, M., Hallett, M., 2006. Modeling the current distribution during transcranial direct current stimulation. Clin. Neurophysiol. 117 (7), 1623–1629.
Naue, N., Rach, S., Strüber, D., Huster, R. J., Zaehle, T., Körner, U., Herrmann, C. S., 2011. Auditory event-related response in visual cortex modulates subsequent visual responses in humans. J. Neurosci. 31 (21), 7729–7736.
Nitsche, M. A., Paulus, W., 2000. Excitability changes induced in the human motor cortex by weak transcranial direct current stimulation. J. Physiol. 527, 633–639.
Nowak, L. G., Bullier, J., 1998. Axons, but not cell bodies, are activated by electrical stimulation in cortical gray matter I. evidence from chronaxie measurements. Exp. Brain Res. 118, 477–488.
Nunez, P. L., Wingeier, B. M., Silberstein, R. B., 2001. Spatial-temporal structures of human alpha rhythms: theory, microcurrent sources, multiscale measurements, and global binding of local networks. Hum. Brain Mapp. 13 (3), 125–164.
Olesch, J., Ruthotto, L., Kugel, H., Skare, S., Fischer, B., Wolters, C. H., 2010. A variational approach for the correction of field-inhomogeneities in EPI sequences. SPIE Medical Imaging: Imag Proc 7623(1), 1–8.
Plonsey, R., Heppner, D., 1967. Considerations on quasi-stationarity in electro-physiological systems. Bull. math. Biophys. 29, 657–664.
Rice, D. M., Hagstrom, E. C., 1989. Some evidence in support of a relationship between human auditory signal-detection performance and the phase of the alpha cycle. Perc. Mot. Skills 69(2), 451–457.
Rodin, E. A., Rodin, M. J., 1995. Dipole sources of the human alpha rhythm. Brain Topogr. 7(3), 201–208.
Romei, V., Gross, J., Thut, G., 2010. On the role of prestimulus alpha rhythms over occipito-parietal areas in visual input regulation: correlation or causation? J. Neurosci. 30(25), 8692–8697.
Romei, V., Gross, J., Thut, G., 2012. Sounds reset rhythms of visual cortex and corresponding human visual perception. Curr. Biol. 22, 1–7.
Rullmann, M., Anwander, A., Dannhauer, M., Warfield, S., Duffy, F., Wolters, C., 2009. EEG source analysis of epileptiform activity using a 1 mm anisotropic hexahedra finite element head model. NeuroImage 44 (2), 399–410.
Sadleir, R. J., Vannorsdall, T. D., Schretlen, D. J., Gordon, B., 2010. Transcranial direct current stimulation (tDCS) in a realistic head model. NeuroImage 51, 1310–1318.
Schroeder, C. E., Lakatos, P., 2009. Low-frequency neuronal oscillations as instruments of sensory selection. Tr. Neurosci. 32 (1), 9–18.
Sejnowski, T. J., Paulsen, O., 2006. Network oscillations: emerging computational principles. J. Neurosci. 26 (6), 1673–1676.
Smith, S. M., 2002. Fast robust automated brain extraction. Hum. Brain. Mapp. 17 (3), 143–155.
Thut, G., Miniussi, C., 2009. New insights into rhythmic brain activity from TMS-EEG studies. Tr. Cogn. Sci. 13 (4), 182–189.
Thut, G., Veniero, D., Romei, V., Miniussi, C., Schyns, P., Gross, J., 2011. Rhythmic TMS causes local entrainment of natural oscillatory signatures. Curr. Biol. 21(14), 1176–1185.
Tuch, D. S., Wedeen, V. J., Dale, A. M., George, J. S., Belliveau, J. W., 2001. Conductivity tensor mapping of the human brain using diffusion tensor MRI. Proc. Natl. Acad. Sci. 98(20), 11697–11701.
Uhlhaas, P. J., Haenschel, C., Nikolič, D., Singer, W., 2008. The role of oscillations and synchrony in cortical networks and their putative relevance for the pathophysiology of schizophrenia. Schiz Bull 34 (5), 927–943.

VanRullen, R., Koch, C., 2003. Is perception discrete or continuous? J. Cogn. Neurosci. 7(5), 207–123.
Varela, F., Lachaux, J. P., Rodriguez, E., Martinerie, J., 2001. The brainweb: phase synchronization and large-scale integration. Nat. Rev. Neurosci. 2(4), 229–239.
Varela, F. J., Toro, A., John, E. R., Schwartz, E. L., 1981. Perceptual framing and cortical alpha rhythm. Neuropsychologia 19, 675–686.
Wagner, T., Fregni, F., Fectau, S., Grodzinsky, A., Zahn, M., Pascual-Leone, A., 2007. Transcranial direct current stimulation: a computer-based human model study. NeuroImage 35, 1113–1124.
Weisz, N., Hartmann, T., Müller, N., Lorenz, I., Obleser, J., 2011. Alpha rhythms in audition: cognitive and clinical perspectives. Front. Psychol. 2:73.
Wolters, C. H., Anwander, A., Berti, G., Hartmann, U., 2007a. Geometry-adapted hexahedral meshes improve accuracy of finite element method based EEG source analysis. IEEE Trans Biomed Eng 54(8), 1446–1453.
Wolters, C. H., Köstler, H., Möller, C., Härdtlein, J., Grasedyck, L., Hackbusch, W., 2007b. Numerical mathematics of the subtraction method for the modeling of a current dipole in EEG source reconstruction using finite element head models. SIAM J Sci Comput 30(1), 24–45.
Wolters, C. H., Kuhn, M., Anwander, A., Reitzinger, S., 2002. A parallel algebraic multigrid solver for finite element method based source localization in the human brain. Comput Vis Sci 5(3), 165–177.
Zaehle, T., Rach, S., Herrmann, C. S., 2010. Transcranial alternating current stimulation enhances individual alpha activity in human EEG. PLoS One 5(11), e13766.
Zhang, Y., Brady, M., Smith, S., 2001. Segmentation of brain MR images through a hidden markov random field model and the expectation maximization algorithm. IEEE Trans Med Imaging 20(1), 45–57.